

Potential-energy surfaces and their dynamic implications

Keiji Morokuma, Qiang Cui and Zhiwei Liu

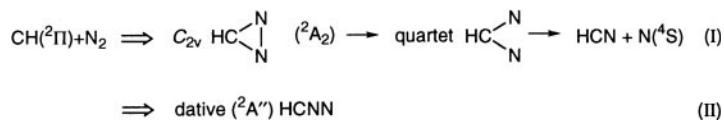
Cherry L. Emerson Center for Scientific Computation and Department of Chemistry,
Emory University, Atlanta, GA 30322, USA

Accurate density functional and *ab initio* calculations have been performed to study the potential-energy surfaces (PESs) and their implications for kinetics and dynamics of: (1) the spin-forbidden reaction $\text{CH}(^2\Pi) + \text{N}_2 \rightarrow \text{HCN} + \text{N}(^4\text{S})$; PES characteristics are calculated and used to evaluate the overall rate using non-adiabatic transition-state theory. (2) Gas-phase ion–molecule reactions: $\text{C}_2\text{H}_2^+ + \text{NH}_3$; PESs are calculated and the mechanism of efficient charge transfer and proton transfer competing with stable complex formation is discussed. $\text{C}_2\text{H}_2^+ + \text{CH}_4$; the mode-enhancement effect has been elucidated in terms of the new transition state and by direct trajectory calculations.

1 Spin-forbidden reaction $\text{CH}(^2\Pi) + \text{N}_2$

The reaction: $\text{CH}(X^2\Pi) + \text{N}_2 \rightarrow \text{HCN} + \text{N}(^4\text{S})$ is a very important reaction in combustion chemistry and is believed to be the key step in the production of NO in hydrocarbon flames.¹ The pressure and temperature dependences of the reaction rate indicate that the reaction proceeds *via* formation of a long-lived complex, and that different mechanisms dominate at low and high temperatures, respectively.²

The PESs for this reaction have been studied by many, including Manna and Yarkony,³ Martin and Taylor⁴ and Walch.⁵ It has been established from these studies that the mechanism of the reaction can be summarized as:



No barrier exists between the reactants and the dative minimum, while a *ca.* 0.7 eV barrier exists between the reactants and the C_{2v} minimum. A large barrier exists between the dative and the C_{2v} structure and, therefore, isomerization between the two does not happen directly. A 2D model potential surface for the channel involving the C_{2v} doublet minimum has been constructed by Walsh and Seideman and used for calculations of the cumulative reaction probability, $N(E)$, and the thermal rate constant.⁶

It would be very useful to have a simple expression for the non-adiabatic reaction rate constant as the standard transition-state theory (TST) for the adiabatic reaction. Such an idea has been discussed by a few authors in a different context.⁷ Among those, the work of Lorquet *et al.*^{7a} is the closest to the extension we plan to make here.

1.1 PESs

There still remain some uncertainties on the barrier heights as well as the energetics of the crossing point. Some structures are found to be not directly connected and some

intermediates are missing. Therefore, we have, first, carried out high-level *ab initio* calculations of the structures and energies of the minima, transition states and the minimum on the seam of crossing (MSX). The structures were optimized and vibrational frequencies were calculated at the B3LYP/6-311G(d,p) level and the energies were recalculated at the G2M(RCC) level.⁸

The global potential-energy profile for the present system thus calculated is shown in Fig. 1. The two dative complexes, HCNN, **d1** in ${}^2A''$ and **d1-2** in ${}^2A'$, have been found, of which **d1** is the ground state. No encounter barrier exists from the reactants to either **d1** or **d1-2**. The path leading to the other type of CHN_2 complex, the so-called C_{2v} complex **d3** (2A_2), as explored by Walch,⁵ goes over a C_1 transition state **d4-ts** to a C_s intermediate **d4** (${}^2A'$), which is converted to a stable complex **d3** (2A_2) after a small barrier at **d3-d4-ts**. As pointed out by Martin,⁴ a large barrier exists at the transition state **d2-ts** (${}^2A''$) for isomerization between **d1** and **d3**.

The quartet state potential-energy profile can also be divided into two different regions: the dative region and the C_{2v} region. The C_{2v} region includes the well-characterized minimum **q3**(4B_1) and the transition state **q3-ts** (${}^4A''$) for dissociation to $\text{HCN} + \text{N}({}^4S)$. They can be accessed at relatively low energy only through intersystem crossing from the doublet state surface in the C_{2v} region. $\text{HCN} + \text{N}({}^4S)$ can be formed directly from the quartet reactants of $\text{CH}({}^4\Sigma^-) + \text{N}_2$ via the two energetically similar *trans* and *cis* dative pathways, via encounter transition states, **q1-ts-cis** and **q1-ts-trans**, through dative minima, **q2-cis** and **q2-trans**, and dissociation transition states, **q2-ts-cis** and **q2-ts-trans**.

The optimized MSX between doublet (2A_2) and quartet (4B_1), **MSX-dq3**, is very close to that of Yarkony.³ At the G2M(RCC) level without ZPE, the energy of **MSX-dq3** is nearly the same as the doublet reactants. The search for MSX for the dative channel between ${}^2A''$ and ${}^4A''$ converged to a structure very close to the *trans*-minimum on the quartet state surface, **q2-trans**. Judging from the higher energy of **q2-trans**, the high exit barrier at **q2-ts-cis** or *trans* and the smaller spin-orbit coupling element (calculated at the CASCF level with the one-electron Breit-Pauli Hamiltonian and empirically fit nuclear charge) between ${}^2A''$ and ${}^4A''$, the dative intersystem crossing channel is not likely to compete with the C_{2v} intersystem crossing mechanism.

In the rate constant calculations with non-adiabatic TST to be discussed below, frequencies of vibrations orthogonal to the norm of the seam at the MSX have to be calculated. The vibrational frequencies at the MSX for the doublet and the quartet states were found to differ by up to as much as 20%. Much tighter convergence criteria⁹ did not reduce the difference, and the difference in the projected vibrational frequencies of the two electronic states comes intrinsically from the definition of the norm of the seam, which is expressed as the energy difference gradient, and causes some errors on the degeneracy condition starting from the second order.

1.2 Non-adiabatic TST

As is well established, the central issue in the rate constant calculations is the derivation of the cumulative reaction probability, $N(E)$, which, within the framework of classical mechanics, is defined as the following:¹⁰

$$N(E) = 2\pi\hbar(2\pi\hbar)^{-F} \int dp \int dq \delta[E - H(p, q)]F(p, q)\chi(p, q) \quad (1)$$

where $H(p, q)$ is the classical Hamiltonian of the molecular system. The flux operator $F(p, q)$ is defined in terms of a dividing surface f which, in most cases, is a function of the

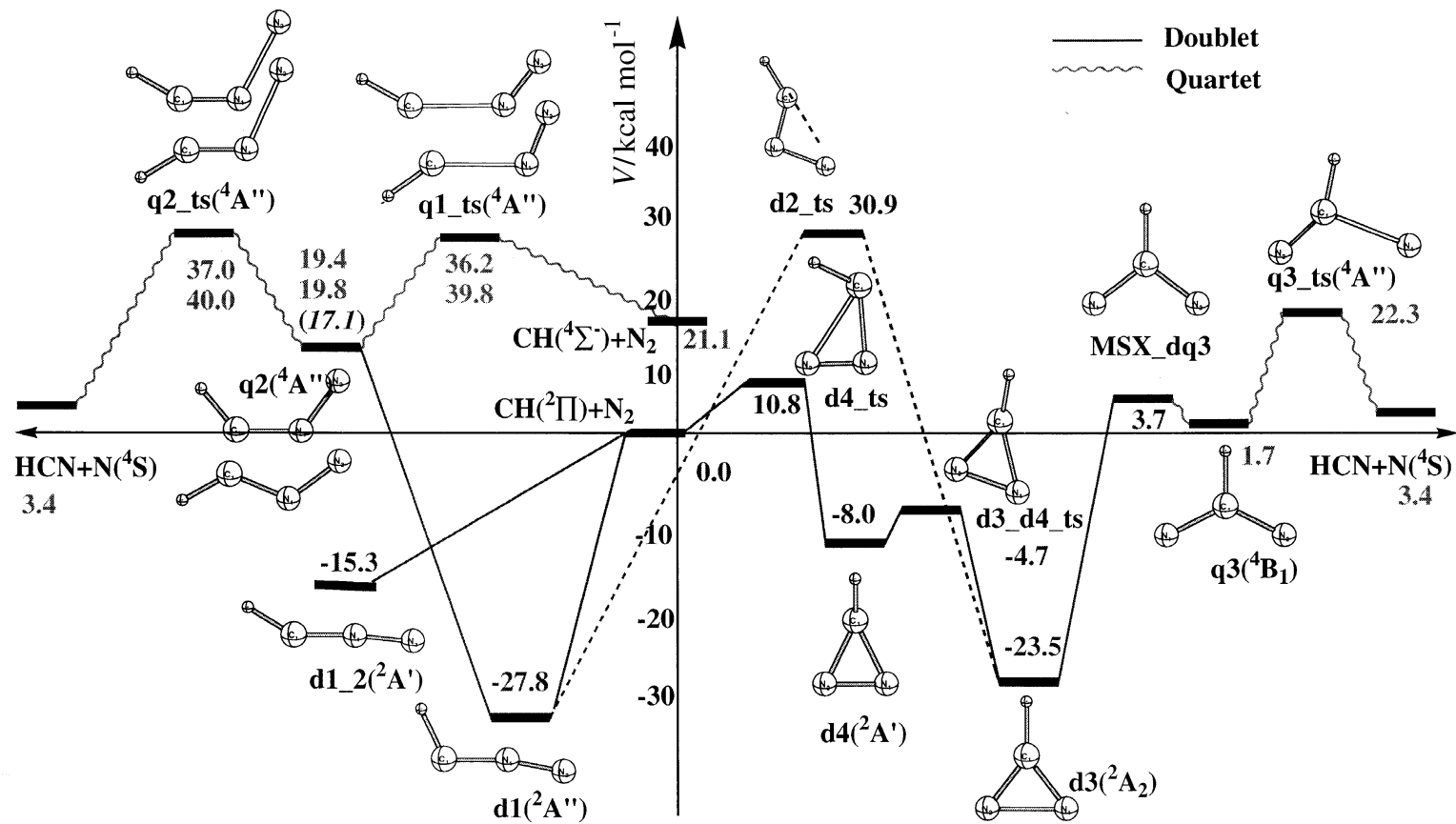


Fig. 1 Global potential-energy profile for the reaction: $\text{CH}(^2\Pi) + \text{N}_2 \rightarrow \text{HCN} + \text{N}(^4\text{S})$. Energies are calculated with G2M(RCC) including ZPC[B3LYP/6-311G(d,p)].

coordinate. To calculate $N(E)$ within a TST framework, one has to obtain the following quantities: (i) the definition of the dividing surface; (ii) the reaction coordinate; (iii) the Hamiltonian in terms of the reaction coordinate and those orthogonal to it and (iv) the characteristic function. We will define these for a non-adiabatic extension of the TST.

(i) Expression of the dividing surface. In the standard TST, one uses the hypersurface that is perpendicular to the reaction coordinate and contains the saddle point: $q_F = 0$. In the present non-adiabatic extension, we choose the seam of crossing as the dividing surface, and use a simple Taylor expansion of the two PESs around the MSX.

Let us start by recalling the definition and a few geometrical properties of the MSX. Let $V_1(\mathbf{q})$ and $V_2(\mathbf{q})$ be the two PESs, which behave like diabatic states in the usual sense owing to their different space \times spin symmetries. The \mathbf{q} s are the mass-weighted Cartesian coordinates. The seam surface can be defined with the simple equation:

$$V_1(\mathbf{q}) - V_2(\mathbf{q}) = 0 \quad (2)$$

Expanding both $V_1(\mathbf{q})$ and $V_2(\mathbf{q})$ up to the first order, we may write

$$[V_1(\mathbf{q}_0) - V_2(\mathbf{q}_0)] + \Delta\mathbf{q} \cdot [g_1(\mathbf{q}) - g_2(\mathbf{q})] \Big|_{\mathbf{q}_0} = 0 \quad (3)$$

Clearly, the norm of the seam surface is nothing but the normalized energy difference gradient,

$$\hat{s} = \frac{\Delta g_{12}(\mathbf{q})}{|\Delta g_{12}(\mathbf{q})|} \Big|_{\mathbf{q}_0}.$$

In the following, \hat{s} is used to denote the normalized vector, and s is used to denote the actual numerical value of the displacement along \hat{s} . The MSX is defined by eqn. (3) and the condition of the minimum on the seam of crossing:

$$(\hat{I} - \hat{s}\hat{s})g_i(\mathbf{q}) = \tilde{\mathbf{0}} \quad (4)$$

As discussed by many authors including us, it is straightforward to set up a Newton–Raphson optimization scheme to locate the MSX with those two constraints.^{11–13} Since the MSX is a true minimum on the seam of crossing, it is valid to make a harmonic expansion around the MSX on the seam of crossing. Following Miller’s reaction path Hamiltonian,¹⁴ one can achieve this by diagonalizing a projected Hessian matrix:

$$\mathbf{H} = (\hat{I} - \hat{P})\mathbf{H}(\hat{I} - \hat{P}) \quad (5)$$

where the projector \hat{P} contains the normal vectors corresponding to the infinitesimal total translation, rotation, and the energy difference gradient vector \hat{s} .

At the MSX, it is well known that the gradient vectors of the two electronic states are either parallel or anti-parallel.¹⁵ Therefore, the \hat{s} vector is parallel or anti-parallel to the gradient of each PES, and the projector in eqn. (5) becomes exactly the same as that in the case of the reaction-path Hamiltonian. Therefore, one can calculate the projected vibrational frequencies at the MSX directly with any *ab initio* package that can handle reaction-path frequency calculations. Since the degeneracy condition is up to first order, the error starts from the second order, which implies that the projected vibrational frequencies for the two electronic states involved will not be exactly the same, as shown in Section 1.1.

From the normal mode analysis on the seam, one obtains $(3N - 7)$ non-zero eigenvalues corresponding to the bound motion on the seam surface, and seven zero eigenvalues corresponding to the total translation/rotation, and the norm of the seam surface. One also obtains a new set of orthonormal coordinate $\{\mathbf{Q}\}$, which are also orthogonal to \hat{s} . With this new set of coordinates, the two diabatic potentials can then be expressed

as:

$$V_i(\mathbf{q}) \equiv V_i(s, \mathbf{Q}) = V_i(s) + \frac{1}{2} \sum_k \omega_k^2(0) Q_k^2(0) \quad (6)$$

and the dividing surface can be expressed by the simple equation

$$s = (\mathbf{q} - \mathbf{q}_0) \cdot \hat{s} = 0 \quad (7)$$

(ii) The ‘hopping’ coordinate. It is natural to choose \hat{s} to be the reaction coordinate, or more appropriately the hopping coordinate. We should emphasize that in most realistic reactions, the hopping coordinate is not the coordinate that leads to the products. Therefore, the $N(E)$ one calculates at the MSX may only be a component of the total rate constant. One usually has to consider the reaction as a multi-step process, and derive the rate constant for the entire reaction with the $N(E)$ s calculated at several critical structures. The reaction of $\text{CH} + \text{N}_2$ is a very typical example, as we shall discuss in Section 1.3.

(iii) System Hamiltonian. The system Hamiltonian can then be expressed as:

$$H_i = \frac{p_s^2}{2} + V_i(s) + \sum_k \left[\frac{p_k^2}{2} + \frac{1}{2} \omega_k^2 Q_k^2 \right] \quad (8)$$

(iv) The characteristic function. The characteristic function for a non-adiabatic process is clearly just a probability factor that the system makes a transition from one diabatic surface to the other:

$$\chi_r(\sqrt{2E_s}, \mathbf{Q}) = P_{\text{tr}}(\sqrt{2E_s}, \mathbf{Q}) \quad (9)$$

In the standard TST, all the trajectories with momenta pointing towards products are counted in the rate expression. In a non-adiabatic process, the trajectory with momenta pointing towards the reactants can also make diabatic transitions and contribute to the rate constant. Therefore, in the weak coupling limit, no Heaviside function of the momentum appears in eqn. (9).

With the definition of necessary ingredients above, one can carry out the integration over s and p_s and obtain the following:

$$N(E) = 2 \times (2\pi\hbar)^{-(F-1)} \int d\mathbf{p}_Q \int d\mathbf{Q} h[E - H^{F-1}(\mathbf{p}_Q, \mathbf{Q})] \chi_r(\sqrt{2E_s}, \mathbf{Q}) \quad (10)$$

where the characteristic function depends, in general, on the energy in the s degree of freedom $E_s = E - H_{F-1}$, and also on \mathbf{Q} . The factor 2 comes from the fact that the flux of both directions can contribute to the rate constant.

The evaluation of the phase-space integral in eqn. (10) can be rather complicated if one considers the transition probability as a function of \mathbf{Q} coordinates. Great simplification can be achieved if we consider the transition probability only as a function of energy in the hopping coordinate. Rewriting the Heaviside function as the integral of a δ function we can write eqn. (10) as:

$$\begin{aligned} N(E) &= 2 \times (2\pi\hbar)^{-(F-1)} \int_0^{E-E_c} dE_s \chi_r(E_s) \int d\mathbf{p}_Q \int d\mathbf{Q} \delta[E - E_c - E_s - H^{F-1}(\mathbf{p}_Q, \mathbf{Q})] \\ &\equiv 2 \times \int_0^{E-E_c} dE_v P_{\text{tr}}(E - E_c - E_v) \rho_{F-1}(E_v) \end{aligned} \quad (11)$$

where E_c is the energy of the MSX, and E_v denotes the energy in the ‘bound’ modes on the seam. The physical meaning is very clear, $N(E)$ is nothing but a weighted sum of density of states at the MSX. The quantum mechanical correspondence of eqn. (11)

is given as:

$$N(E) = 2 \times \sum_{\{n\}} P_{\text{tr}}(E - E_{v\{n\}}) \quad (12)$$

1.3 Application of non-adiabatic TST to the reaction

We would like to apply the non-adiabatic TST described above to the reaction rate of the reaction: $\text{CH}({}^2\Pi) + \text{N}_2 \rightarrow \text{HCN} + \text{N}({}^4\text{S})$, using the potential-energy properties calculated *ab initio* in Section 1.1. In the current study, we have employed the simplified reaction mechanism,⁶ as illustrated in Fig. 2, without considering the dative channel. The entire process of $\text{CH}({}^2\Pi) + \text{N}_2 \rightarrow \text{HCN} + \text{N}({}^4\text{S})$ is divided into three stages: (i) overcoming the barrier **d4-ts** to form **d3**; (I) intersystem crossing from the doublet **d3** to the quartet state **q3** through the region around **MSX-dq3**; and (ii) overcoming the barrier **q3-ts** to form the quartet product $\text{HCN} + \text{N}({}^4\text{S})$. We treat each step independently and finally combine them to obtain the rate constant from the whole process using the unified statistical theory (UST) of Miller,¹⁶ noting that we have two rather deep and long-lived complexes **d3** and **q3**. $N(E)$ for the rate constant for the total spin-forbidden reaction process is obtained as the following in terms of the $N(E)$ at each critical structure:

$$N_0(E) = \frac{N_1 N_2 N_3 N_x N_y}{(N_2 N_y + N_3 N_y - N_2 N_3)(N_2 N_x + N_1 N_x - N_2 N_1)} \quad (13)$$

Here, as illustrated in Fig. 2, 1, 2, and 3 denote the first, second and third transition states, respectively, and x and y denote the first and second complexes, respectively.

In the calculation according to eqn. (13), we have used harmonic direct counting to calculate all the $N_i(E)$ s. To calculate the $N_2(E)$ at **MSX-dq3**, we used the calculated projected vibrational frequencies. In order to calculate the transition probability, another ingredient in the calculation of $N_2(E)$, as a function of energy in the hopping

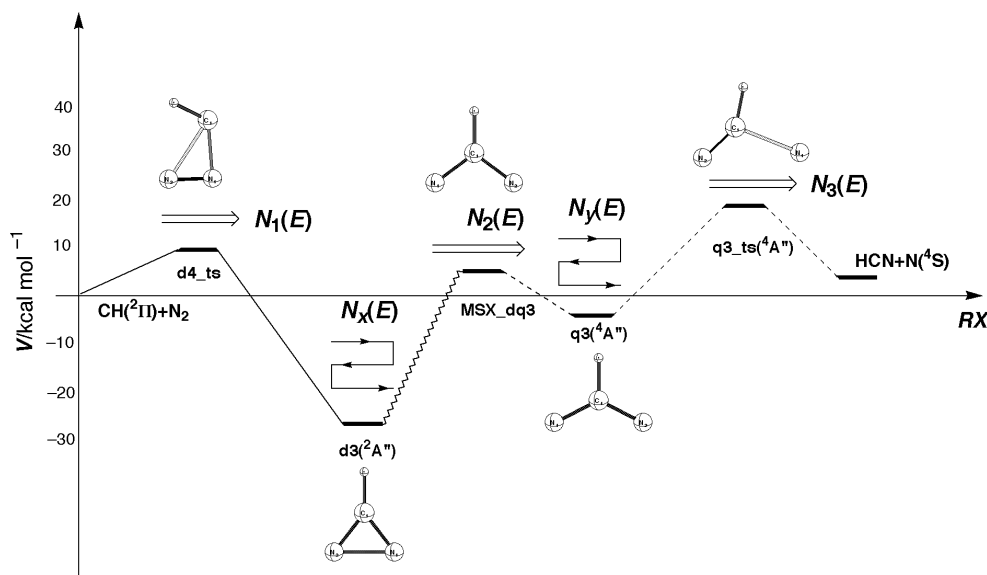


Fig. 2 Simplified schematic potential-energy profile for the reaction: $\text{CH}({}^2\Pi) + \text{N}_2 \rightarrow \text{HCN} + \text{N}({}^4\text{S})$ used in the rate constant calculations

coordinate \hat{s} , we first had to establish a 1D model. We carried out CASPT2/6-311G(d,p) along the N—C—N bending coordinate from **d3** to **q3**, with other parameters fixed at those of **MSX-dq3**. We used the spin-orbit coupling elements calculated in Section 1.1. To carry out $N_2^{1d}(E)$ calculations quantum mechanically, we artificially flattened out the potential-energy curves of the doublet (quartet), when the N—C—N angle was smaller (larger) than that in the **d3(q3)** to model the asymptote. Furthermore, we also made the doublet artificially steeper after the N—C—N angle was close to that in **q3**. The goal was to calculate the transition probability which was only affected by a very small portion of the PESs near the MSX. Even with these artificial modifications, the model is still far better than the linear potential-constant coupling model assumed in many transition formulae. After the 1D model was established, the distorted wave approximation (DWA) was used to calculate the transition amplitude (the square root of the transition probability):

$$T_{oi} \equiv \sqrt{P_{oi}} = 2(k_o k_i)^{-1/2} \int_0^\infty \psi_i^{(0)}(r') V_{io}(r') \psi_o^{(0)}(r') dr' \quad (14)$$

where $V_{io}(r)$ is the diabatic coupling element.

The parameters obtained in the *ab initio* calculations and used in the non-adiabatic TST calculations are shown in Table 1. The calculated transition probability $N_2^{1d}(E)$, thus calculated as a function of energy is presented in Fig. 3(a). Evidently, the DWA exhibits oscillations in the transition probabilities, which manifest as interference between the trajectories on the two diabatic surfaces. The absolute value of the transition probability is very small, of the order of 10^{-4} ; the reaction is very ‘diabatic’ in the MSX region. To examine if the numerical value of $N_2^{1d}(E)$ is consistent with the 2D $N_2^{2d}(E)$ obtained by Seideman,^{6b} we convoluted $N_2^{1d}(E)$ with the asymmetric C—N stretch vibrational frequency at **MSX-dq3** (943 cm^{-1} , which is 1005 cm^{-1} for the quartet state). The derived result, denoted as $N_2^{2d}(E)$, plotted in Fig. 3(b), is of the order of 10^{-3} , and exhibits some moderate oscillations, much less sharp than those of Seideman’s $N_2^{2d}(E)$.

With the obtained $N_2^{1d}(E)$, we then calculated $N(E)$ and $k(T)$ for the whole reaction. $N(E)$ for $J = 0$ is shown in Fig. 3(c). Even after convolution of the five vibrational degrees of freedom, $N(E)$ shows structures which are more visible when the ${}^2A''$ frequencies at **MSX-dq3** are employed in the calculations. In addition, $N(E)$ obtained with the ${}^4A''$ frequencies is larger than that calculated with the ${}^2A''$ frequencies, as the numerical values of the frequencies are generally smaller for the former. The transition probability at **MSX-dq3** is so small that the total $N_o(E)$ is reduced to $N(E)$ at **MSX-dq3**. Since **MSX-dq3** is the rate-determining structure, we have simply employed J -shifting to derive the thermal rate constant. The resultant $k(T)$ in the temperature range of 1000–3000 K, shown in Fig. 3(d), can be fitted to an Arrhenius expression with a prefactor of $10^{9.19}$, which seems to be too low compared with recent experimental measurements and an empirical RRKM study, which has a prefactor of *ca.* 10^{11-12} .

Comparing our results with the previous empirical RRKM study of Rogers *et al.*¹⁷ [$k_{\text{fit}}(T)$ in Fig. 3(d)], we note that they mentioned that a much smaller rate constant is obtained compared with experimental measurement unless several empirical frequencies are scaled down by a factor of 2 and a very large κ value of 0.04 (larger than the L—Z probability 0.001–0.01 of Yarkony *et al.*) is used to describe the intersystem crossing probability. Indeed, the scaled results contain three frequencies around 300 cm^{-1} , much lower than the *ab initio* frequencies we have obtained. With their vibrational frequencies, we found that our rate constant increased by more than an order of magnitude. Further, assuming that the spin-orbit coupling element is two times larger than we have calculated, the derived thermal rate constant becomes $k_2(T)$ in Fig. 2(d).

Obviously, scaling the frequencies and coupling element is not a solution but, rather, it strongly suggests that some important issues may have been overlooked and require

Table 1 Parameters used in the non-adiabatic TST calculation for the reaction of CH + N₂

structure	frequencies ^a /cm ⁻¹	energetics ^b /cm ⁻¹	$I^a/u a_0^2$	μ_{1D}^c
CH ₂ (² Π), N ₂	2804.3, 2447.0	0.0	4.2, 30.0	
d4-ts (² A)	300.9, 600.4, 1036.2, 1900.7, 3008.2	4932	52.2, 19.9, 14.6	
d3 (² A ₂)	718.1, 838.7, 926.3, 1193.3, 1636.4, 3206.2	-7310	41.4, 29.1, 17.1	
MSX-dq3 (² A ₂)	943.2, 948.3, 1370.7, 1476.0, 3025.8	1609	63.5, 16.6, 13.2	16242.8
MSX-dq3 (⁴ B ₁)	797.4, 1005.0, 1059.7, 1358.6, 3040.8	1600	63.5, 16.6, 13.2	
q3 (⁴ B ₁)	562.0, 809.1, 1103.4, 1187.4, 1225.2, 2886.5	-700	98.0, 13.1, 11.5	
q3-ts (⁴ A'')	349.2, 741.1, 866.2, 1929.5, 3294.6	6401	68.2, 10.0, 8.7	

^a Derived from the B3LYP/6-311G(d,p) results. ^b Derived from the UCCSD(T)/6-311G(d,p) results. ^c Reduced mass in the 1-D effective Hamiltonian, in au.

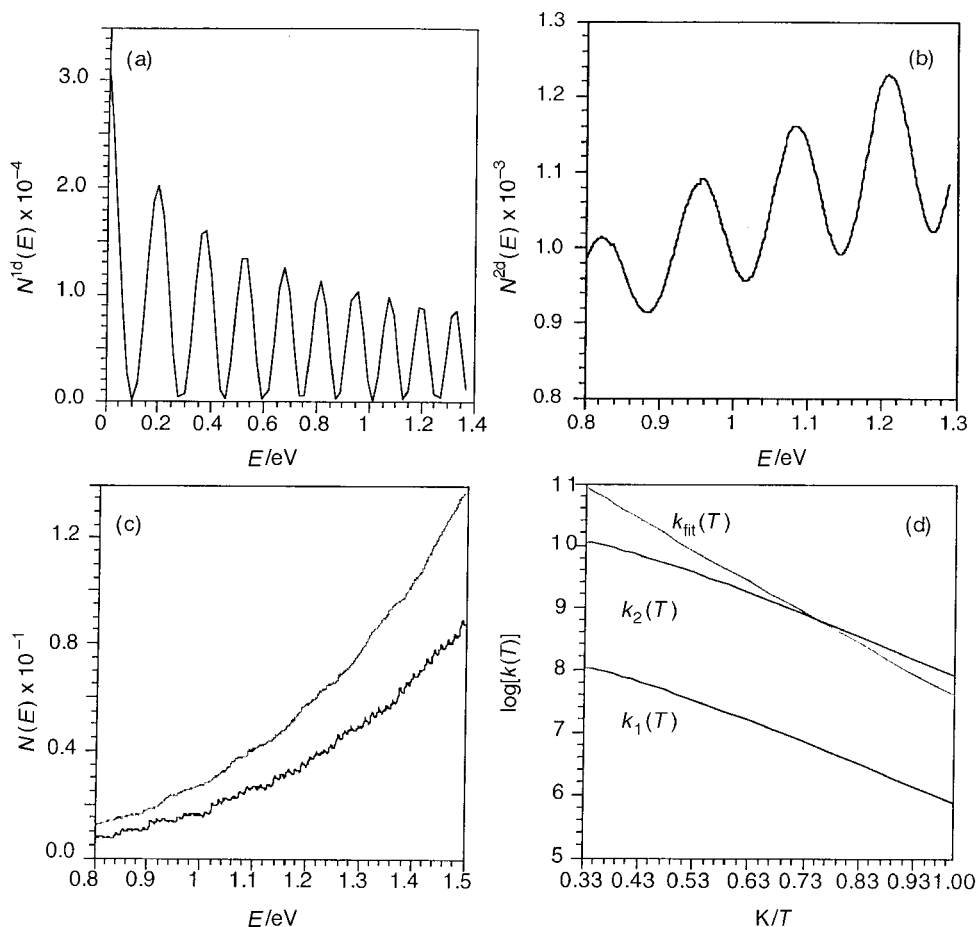


Fig. 3 (a) 1D transition probability obtained with the distorted wave approximation as a function of energy. (b) 2D cumulative reaction probability $N_2^{2d}(E)$ obtained by energy shifting approximation based on $N_2^{1d}(E)$ as a function of energy. The frequency for the bound degree of freedom is selected to be the asymmetric C—N stretch of the $^2A''$ state at **MSX-dq3**. (c) $N_0(E)$ for the total reaction calculated according to eqn. (13). The relatively smooth curve is obtained with the set of vibrational frequencies for the $^4A''$ state at **MSX-dq3**, and the curve with more visible structures is calculated with the $^2A''$ frequencies at **MSX-dq3**. (d) Calculated thermal rate constant $k_1(T)$ for the production of quartet products. $k_2(T)$ is computed with scaled vibrational frequencies of **MSX-dq3** from ref. 17 and two-fold larger spin-orbit coupling constant. $k_{fit}(T)$ is from ref. 17.

further investigation. For instance, although a 1D model for the intersystem crossing sounds very reasonable, judging from the structure of **d3**, **MSX-dq3** and **q3**, it is possible that another degree of freedom, possibly the C—N stretch, is also crucial to the spin-forbidden transition. By this we mean that the transition probability χ , which in the current work is assumed to depend only on the energy in the hopping coordinate, might actually vary significantly along one or more degree of freedom orthogonal to the norm of the seam s . We note that at the **q3** structure, the doublet electronic state is not very high in energy and, therefore, the seam might cover a larger region of the PES at a certain energy than that based on simple harmonic expansion at **MSX-dq3**. Indeed, as we mentioned above, $N^{2d}(E)$ appears to increase too slowly as a function of the energy, compared to the explicit 2D quantum mechanical calculation of Seideman.^{6b} Therefore,

rigorous quantum dynamic calculations with at least two degrees of freedom, with accurate spin-orbit coupling elements in an extended region, together with approximate treatment of other degrees of freedom, are required to examine the situation in more depth.

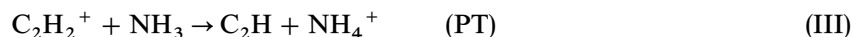
1.4 Conclusions

The detailed reaction mechanism of the spin-forbidden reaction $\text{CH}(^2\Pi) + \text{N}_2 \rightarrow \text{HCN} + \text{N}(^4\text{S})$ has been studied with high-level *ab initio* methods. Although a few new structures have been found on both the doublet and quartet electronic states, the dominant mechanism remains the C_{2v} intersystem crossing mechanism summarized by Walch.⁵ Vibrational frequencies orthogonal to the norm of the seam have been calculated at the MSX and applied to calculate the rate with an extension of the TST for spin-forbidden reactions. A one-dimensional model was set up to consider the spin-forbidden transition probability. The effect of other degrees of freedom was then considered by energy convolution with the vibrational frequencies orthogonal to the seam of crossing at the MSX. The calculated cumulative reaction probability $N(E)$ seems to be consistent with that obtained by Seideman,^{6b} with the ABC-DVR-Fermi-Golden-rule approach and a 2D model. Nevertheless, with such a TST expression and the 1D model for the intersystem crossing process, the thermal rate constant $k(T)$ seems to be too low by two orders of magnitude compared with experimental measurements. Indeed, the vibrational frequencies obtained in the current study are much larger than that from an empirical RRKM study, where empirical vibrational frequencies at the MSX had to be scaled by a factor of two in order to derive a reasonable $k(T)$. Such a discrepancy strongly suggests that some important issues might have been overlooked. In particular, the assumption that the spin-forbidden transition takes place with uniform probability on the seam may be a poor assumption in the particular case we are considering.

2 Dynamics of gas-phase ion-molecule reactions

2.1 $\text{C}_2\text{H}_2^+ + \text{NH}_3$

In the recent experiment by Anderson and co-workers,¹⁸ the only product channels observed over a wide range of collision energy are charge transfer (CT) and proton transfer (PT).



Surprisingly, no evidence for the formation of the stable $\text{C}_2\text{H}_5\text{N}^+$ intermediates has been observed. The H-abstraction channel, which was dominant at high collision energy for the isoelectronic system of $\text{C}_2\text{H}_2^+ + \text{CH}_4$,¹⁹ was also not observed. It is not surprising, for thermodynamic reasons, that the CT and PT channels become open for the NH_3 system than for the CH_4 system. However, the thermodynamic properties of the complex channel and the H-abstraction channel are qualitatively similar for both systems. Therefore, it is really intriguing why these channels have been observed experimentally for $\text{C}_2\text{H}_2^+ + \text{CH}_4$ but not for $\text{C}_2\text{H}_2^+ + \text{NH}_3$ over a wide range of collision energy.

All the observations suggest that PT is a direct channel with a proton-stripping mechanism. As for the CT channel, two different mechanisms seem to exist. At low

energy, CT takes place through a weakly bound complex with a lifetime longer than *ca.* 1 ps. At higher energy, the charge seems to be transferred by a long-range electron hopping mechanism.

Finally, the effect of vibrational excitation in the reactant $C_2H_2^+$ on the reaction has also been examined, as in the study of $C_2H_2^+ + CH_4$, where a large effect has been observed. The effect is much smaller in the present system, albeit very mode-specific.¹⁹ In the PT channel, the reaction is enhanced by $C_2H_2^+$ bending and inhibited by the CC stretch. In the CT channel, both CC stretch and bending in $C_2H_2^+$ inhibit the reaction at high collision energy. At low collision energy, the reaction is inhibited by the CC stretch, but enhanced by the HCC bending in $C_2H_2^+$. All these facts suggest a reaction mechanism where the $C_2H_2^+$ vibration influences the probability of a favourable reactant geometry arrangement, while the branching between product channels is determined later in the collision by factors not strongly dependent on the reactant vibration. However, the origin of the mode-specificity observed remains unclear.

Very little is known about the PESs of the present system, except for some structures of the stable $C_2H_5N^+$ complexes in the ground electronic state.²⁰ In the present study, in order to find the relationship between the potential-energy characteristics and the reaction dynamics, we have performed detailed and highly accurate calculations of the PESs. The overall potential-energy profile calculated at the G2M(RCC)//B3PW91/6-311G(d,p) level, with sketches of some important structures, is shown in Fig. 4.

PT channel. For both the reactants and products of the PT channel, close-lying electronic states exist. For the reactants, $C_2H_2^+(^2\Pi) + NH_3$ is doubly degenerate, with the low lying non-degenerate $C_2H_2 + NH_3^+$ state. For the products, $C_2H(^2\Sigma^+) + NH_4^+$ is the lowest asymptote, with the upper dissociation asymptote $C_2H(^2\Pi) + NH_4^+$ only 0.50 eV higher in energy, and also lower than the reactants of $C_2H_2^+ + NH_3$. If the reaction proceeds from $C_2H_2^+ + NH_3$ with perfect linear N–C–C framework, which is the minimum energy path, PT1, C_{3v} symmetry is maintained during the reaction. In C_{3v} , both $C_2H_2^+(^2\Pi) + NH_3$ and $C_2H(^2\Pi) + NH_4^+$ fall into the doubly degenerate 2E symmetry and are directly correlated. The PT1 channel in the 2E symmetry does not involve any entrance or exit barrier, and proceeds through an intermediate complex, **PT-1**, which resembles the products, $C_2H(^2\Pi) + NH_4^+$, as shown in Fig. 4. Although the 2E state in C_{3v} is subject to Jahn–Teller distortion, in general, the effect is evidently very small in the case of **PT-1**. Although the calculation is carried out in C_s , the A' and A'' states are nearly degenerate, and all the vibrational frequencies are real. This is not unexpected, because the structure of **PT-1** is very product-like. In the experiment, the detection of the velocity distribution of NH_4^+ (or actually its isotopomer ND_3H^+) indicates that the PT channel follows a direct stripping mechanism even at low collision energy. The present channel supports the fast ‘stripping’ mechanism proposed by Anderson and co-workers.

The PT2 channel, on the other hand, proceeds from the ground state of the reactant, $C_2H_2 + NH_3^+$, through a transition state, **PT-TS1**, shown in Fig. 4, and no intermediate is involved. $C_2H_2 + NH_3^+$ and $C_2H(^2\Sigma^+) + NH_4^+$ both fall into the 2A_1 symmetry, and are directly correlated. In the PT2 channel it is actually an H atom that has been transferred. The existence of the barrier in the PT2 channel is not surprising either, since unlike PT processes, most H-atom transfer reactions proceed with barriers. **PT-1** lies 1.41 eV below $C_2H_2^+ + NH_3$, and **PT-TS1** lies 0.77 eV above $C_2H_2 + NH_3^+$.

In addition, we have found an unexpected $^2A'$ TS structure in C_s , **PT-TS2**, as shown in Fig. 4. IRC calculation indicates that **PT-TS2** actually connects intermediate **PT-1** and **CC-1**, a covalent NH_5CHCH^+ complex which will be discussed later. Therefore, the PT channel and the CC channel are now connected *via* **PT-TS2**, which is only 0.30 eV above **PT-1**.

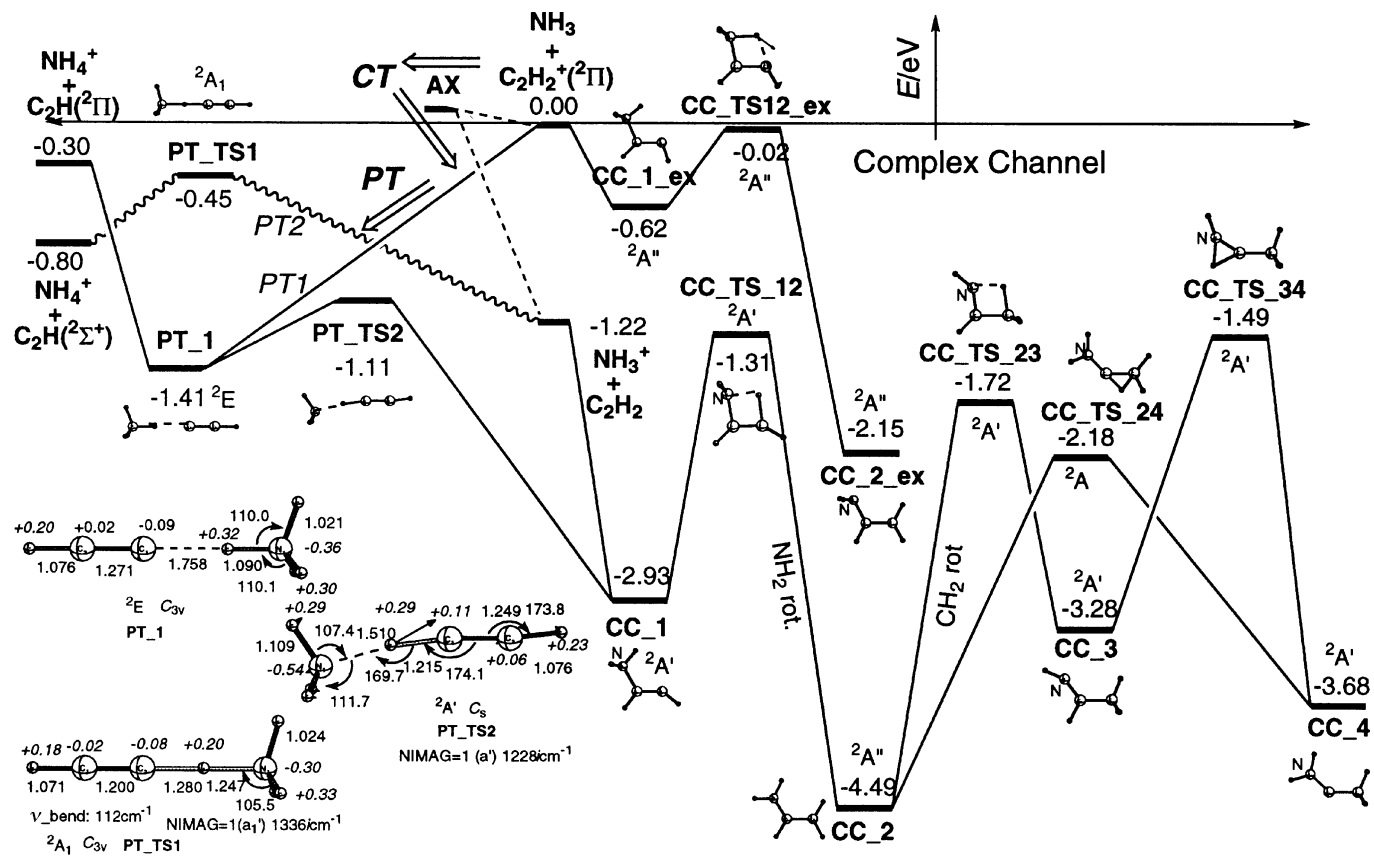


Fig. 4 Overall potential-energy profiles for the reaction of $\text{NH}_3 + \text{C}_2\text{H}_2^+$. Energies are obtained from the G2M//B3PW91/6-311G(d,p) level including ZPE. The B3PW91/6-311G(d,p) optimized geometries (in Å and degrees) of some key structures are also shown.

2.1.2 Covalent $C_2H_5N^+$ complex (CC) formation channel. Several isomers of $C_2H_5N^+$, **CC-1** (NH_3CHCH)⁺, **CC-2** (NH_2CHCH_2)⁺, **CC-3** ($NHCHCH_3$)⁺ and **CC-4** (NH_2CCH_3)⁺, and several isomerization TSs between them, **CC-TS-12**, **CC-TS-23**, **CC-TS-24** and **CC-TS-34**, have been located. The results for the ground electronic-state structures agree well with the previous study,²⁰ except for **CC-1** (NH_3CHCH)⁺ (which connects the Pt channel to the CC channel, as discussed above) and **CC-TS-12**, which seem to have been overlooked previously. No entrance channel barrier has been found on the lowest adiabatic PES, which makes it even more mysterious that no products from the covalent $C_2H_5N^+$ complexes have been found in the experimental work.¹⁸

To rationalize the experimental fact that no CC channel products have been observed, one recognizes that the reactants $NH_3 + C_2H_2^+$ correlate adiabatically to the excited states of these covalent $C_2H_5N^+$ species. Although not very high in energy, the formation of these complexes requires significant alternation of the $C_2H_2^+$ geometry and electronic structure. Therefore, the system is most likely to follow the PT channel instead of visiting the CC formation channel. However, the experimental fact that no products from the CCs have been observed still remains to be a mystery. The fact that no H-abstraction products $NH_2 + C_2H_3^+$ have been observed can be understood similarly, although no calculations have been carried out.

2.1.3 CT channel. For the CT process, two pathways seem to exist according to the different product recoil velocity distribution.¹⁸ Although it is not totally clear from the current study what are these two paths, one may make some speculations. First, one may imagine different crossing structures, depending on the angles of approach of the two fragments. As we have seen in Section 1.3, the two asymptotes $NH_3 + C_2H_2^+$ and $NH_3^+ + C_2H_2$ are rather close in energy at the $NH_3 + C_2H_2^+$ geometry. As the two fragments NH_3^+ and $C_2H_2^+$ approach with large angles, the two $^2A'$ states interact strongly and the $2^2A'$ adiabatic state becomes repulsive. Therefore there exists a good chance for the PES to cross at long separation. CT cannot take place at very far nuclear separation, however, owing to the weak interaction between the electronic states and, therefore, the small coupling element. Consequently, to have a good Franck–Condon factor as well as a reasonably large coupling element, an intermediate-range crossing structure is desired. On the other hand, the situation is rather different when the two fragments approach with small angles, close to linear. In this case, the two $^2A'$ surfaces interact rather weakly owing to their diabatic characters and undergo weakly avoided crossings. As a result, the CT channel for the linear configuration case might yield products with quite different characteristics. In addition, one may also suspect that the two CT paths come from different non-adiabatic processes, namely $A' \rightarrow A'$ CT and $A'' \rightarrow A'$ CT. To have more quantitative results, one needs to optimize the MSX structures for $^2A'/^2A'$, and also $^2A'/^2A''$, probably as a function of the relative angle of approach of the fragments. These calculations have not been carried out in the current study.

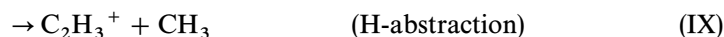
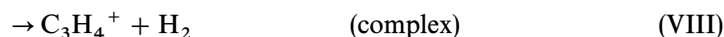
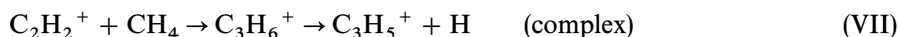
2.1.4 Conclusions. In C_{3v} symmetry where the N–C–C framework is linear, the reactants $NH_3 + C_2H_2^+$ lead to the PT products $NH_4^+ + C_2H(^2\Pi)$, without any barrier, and only through a moderately bound complex which is very product-like. This path supports the fast stripping mechanism proposed by Anderson and co-workers. We have also located, on the $1^2A'$ state surface, a transition state that connects the intermediates in the PT channel to the covalent species **CC-1**. Some trajectories may take this pathway. Several isomers of $C_2H_5N^+$ and the isomerization TSs between them have been located. To rationalize the experimental fact that no CC channel has been observed, we argue that the reactants $NH_3 + C_2H_2^+$ correlate adiabatically to the excited states of these covalent $C_2H_5N^+$ species. Although not very high in energy, the formation of these complexes requires significant alternation of the $C_2H_2^+$ geometry and electronic structure. Therefore, the system is most likely to follow the PT channel rather than

visiting the CC formation channel. However, the experimental fact that no products from the CCs have been observed still remains a mystery. The fact that no H-abstraction products $\text{NH}_2 + \text{C}_2\text{H}_3^+$ have been observed can be understood similarly, although no calculations have been carried out in the current work. For the CT channel, the $^2\text{A}'$ state is repulsive in most regions except around the linear configuration, where the potential energy is attractive and readily leads to CT or PT. The shape of the $1^2\text{A}'$ state confirms the existence of a saddle point between the potential well at the linear configuration and **CC-1**, which has been optimized as **PT-TS2**. The $2^2\text{A}'$ state is mostly repulsive at all angles of approach. CT at different angles of approach, or CT between electronic states of different symmetries, ($\text{A}' \rightarrow \text{A}'$, $\text{A}'' \rightarrow \text{A}'$) may produce final products with different characteristics, and might account for the two pathways proposed by Anderson co-workers.

2.2 $\text{CH}_4 + \text{C}_2\text{H}_2^+$

2.2.1 Mode-enhancement effect. Controlling the outcome of reaction by ‘mode-selective excitation’ concentrates on the local mode, and emphasizes selective excitation of a particular motion, which encourages reaction toward the desired channel.²¹ Many beautiful examples have been accumulated over the years in the photodissociation processes of vibrationally or rovibrationally selected small molecules including H_2O ,^{21a-d} HNCO ,^{21e,f} and C_2H_2 .^{21g}

Recent experiments¹⁹ provide some new examples in the case of more complex ion-molecule reactions that are vibrationally selective. Zare *et al.* studied the reaction of ammonium ion and ND_3 and found that the umbrella mode of NH_3^+ enhances CT and deuterium abstraction significantly, while the isoenergetic excitation of the breathing mode does not induce any effect.^{19c} In another experiment, Anderson and co-workers^{19a,b} have studied the effects of collision energy and mode-selective vibrational excitation on the reaction of C_2H_2^+ with CH_4 and CD_4 via a guided-ion beam scattering instrument. Two distinct reaction mechanisms are active in the energy range below 5 eV. At low energies, a long-lived C_3H_6^+ complex forms efficiently and then decomposes primarily to $\text{C}_3\text{H}_5^+ + \text{H}$ and $\text{C}_3\text{H}_4^+ + \text{H}_2$.



Competing with reactions (7) and (8) is a hydrogen transfer reaction (9), producing $\text{C}_2\text{H}_3^+ + \text{CH}_3$ with little atom scrambling. Channel (IX) is strongly enhanced by collision energy and becomes dominant above 0.4 eV. One interesting feature about this channel is that, while CC stretching provides a weaker enhancement than collision energy, two quanta of C—H bending modes (*ca.* 155 meV) enhance the reaction at least *ca.* ten-fold. Based on the isotope study with CD_4 , they concluded that there exist two possible reaction mechanisms for reaction (9): CH_3 elimination from a long-lived C_3H_6^+ complex and direct H-atom abstraction through an oscillating intermediate, where the latter is dominant by a factor of *ca.* 5–10 : 1. They also predicted an early barrier 150 ± 50 meV. The enhancing effect of the C—H bending mode on the reaction is explained by the necessity of carbon atom rehybridization from sp to sp^2 , thus forming a bent TS during the bonding process.

The amazing experimental results have certainly attracted the attention of theoreticians. A combined quantum and TS theory (TST) study has been carried out by Klippenstein to unravel the detailed reaction mechanism and the observed mode-enhancement effect.²² Based on the structure and frequencies of several intermediates obtained at the level of MP2/6-31G(d) and G2²³ energetics, TST calculation was found to yield qualitatively correct cross-sections for the direct channel (9), but not so satisfac-

tory for the complex channels, (VII) and (VIII). It was found that, if the energetics of the TS involved in the complex channels was lowered by 4.5 kcal mol⁻¹, the magnitude of the cross-section for the complex channel could be qualitatively reproduced. Most importantly, no entrance or exit channel barrier was found for the H-abstraction channel (IX). However, it was found that enhancement of the H-abstraction cross-section by the H—C—C bending excitation in C₂H₂⁺ was qualitatively reproduced if the two quanta of H—C—C bending were assumed to be totally randomized.

It might look as if all the issues have been solved by the work of Klippenstein. However, the necessity of artificially lowering the energy of the TS involved in the complex channel looks somewhat questionable. Judging from the structure of the TS presented in ref. 22, we suspect that there may be a lower saddle point, with totally different structure, involved in the complex channel. In addition, the system might be an ideal one to test the capacity of the direct trajectory method.²⁴ In the present study, we have performed detailed and highly accurate calculations of the PESs and compared these with the previous results. We also performed a few direct trajectory calculations. The overall potential-energy profile calculated at the G2M(RCC)//B3PW91/6-311G(d,p) level, with sketches of some important structures, is shown in Fig. 5.

H-abstraction channel. For the H-abstraction channel, as shown in Fig. 5, there exists no entrance barrier to reach the structure of **abs-1**, the so-called classical CH₄···C₂H₂⁺ minimum, or no exit barrier from **abs-1** to the product, the results are essentially the same as in ref. 22. However, the so-called bridged CH₄···C₂H₂⁺ is a minimum at the MP2/6-31G(d) level, while it is a second-order saddle point **abs-TS1** at the present B3PW91/6-311G(d,p) level, connecting **abs-1** and its pseudo-mirror image **abs-1'**. Optimization at the CCSD(T)/6-31G(d,p) level agrees with the present results, suggesting strongly that B3PW91/6-311G(d,p) is closer to reality than MP2. To summarize, the overall mechanism of the H-abstraction channel is the so-called ‘direct’ abstraction channel, actually proceeding through a moderately bound (*ca.* 15 kcal mol⁻¹) complex without entrance or exit barrier

Covalent C₃H₆⁺ CC channel. In ref. 22 the complex channel (7) and (8) leading to C₃H₆⁺ has been shown to proceed from the so-called classical CH₄···C₂H₂⁺ through a saddle point, **com-TS1-K**, which is also included in Fig. 5. However, with the high energy for this TS, the calculated cross-section is, even qualitatively, too small. Indeed, the structure of **com-TS1-K** does not look like a transition state for C—H activation of CH₄ by C₂H₂⁺, but more like a C₂H₃⁺ isomerization TS between its two conformations, perturbed by a CH₃ fragment. We have actually located a new C₁ transition state **com-TS1**, shown in Fig. 5, which was missed in the previous study.²² The IRC²⁵ calculations verify that this TS actually connects **abs-1** and C₃H₆⁺.

At the G2M level, the energy of **com-TS1** is 0.38 eV (8.7 kcal mol⁻¹) below the reactants, and the barrier height measured from **abs-1** is 0.28 eV (6.5 kcal mol⁻¹). In ref. 22, a qualitatively correct cross-section was obtained by artificially lowering the barrier at **com-TS1-K** from 11.7 to 7.2 kcal mol⁻¹. Therefore, we are confident that with the present results reasonable cross-sections, comparable to the experimentally measured value can be obtained.

Direct trajectory calculations. Our *ab initio* calculations indicate that H—C—C bending is clearly strongly coupled to the reaction path and, therefore, additional energy in this mode may contribute effectively to the reaction rate, while the C—C stretch is nearly inert during the whole reaction. In order to find some characteristics of the dynamical process, we have ran three direct trajectories with the C_s constraint at the B3PW91/6-31G(d,p) level.

In all the trajectories, the impact parameter *b* is taken to be zero, and the initial velocity is along the line that joins the centres of mass of CH₄ and C₂H₂⁺ and is

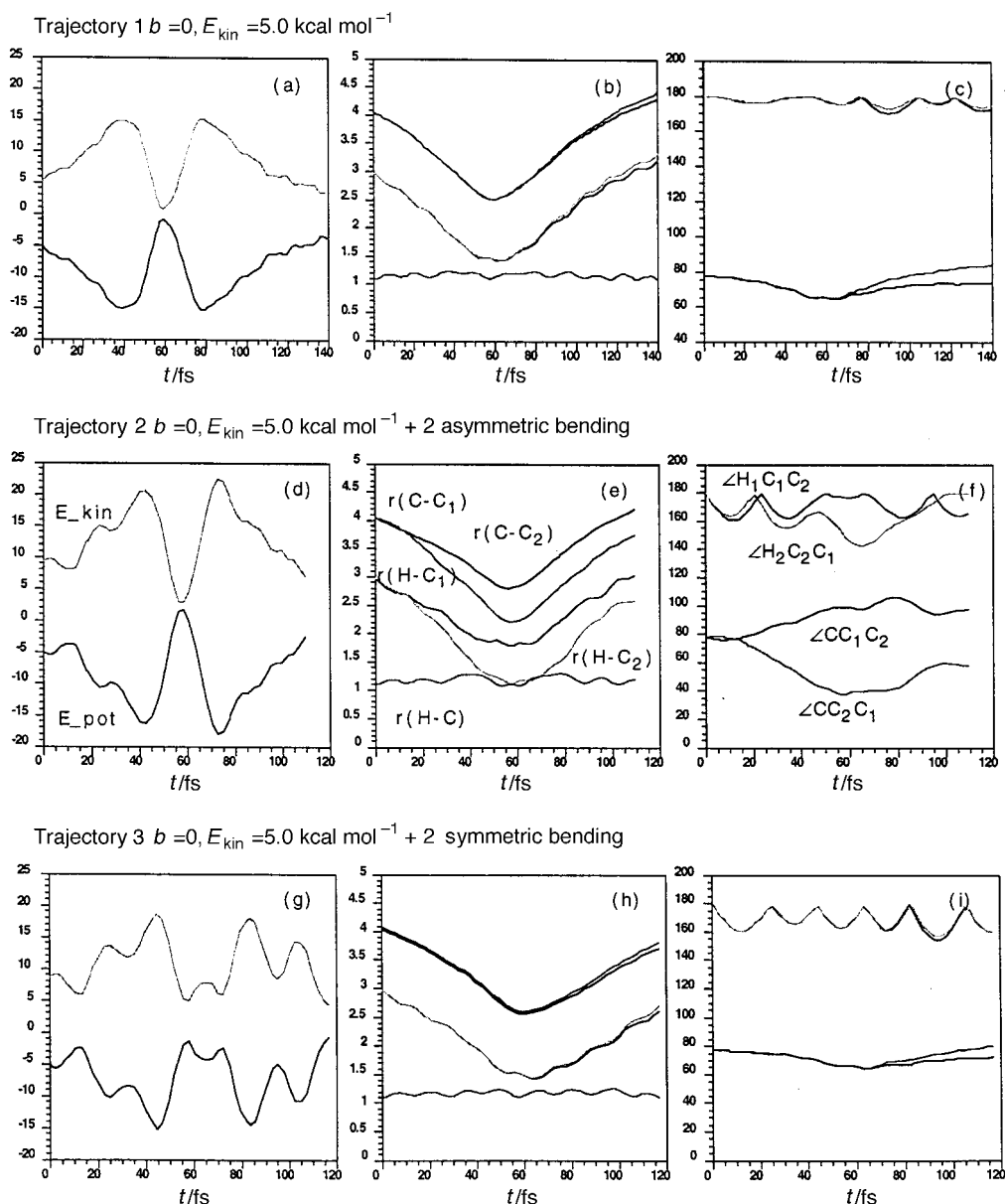


Fig. 6 Results from three direct trajectory calculations for the reaction of $\text{CH}_4 + \text{C}_2\text{H}_2^+$. The first column [(a), (d) and (g)] represents kinetic and potential energies in kcal mol^{-1} . The second [(b), (e) and (h)] and the third column [(c), (f) and (i)] give essential bond distances (in Å) and bond angles (in degrees), respectively, as indicated in the figures.

perpendicular to the CC triple bond in C_2H_2^+ . All the trajectories start with the centre of mass separation of 4.0 Å. In trajectory 1, the initial velocity in the centre of mass frame has been scaled so that the total initial kinetic energy is $5.0 \text{ kcal mol}^{-1}$. In the trajectories 2 and 3, the initial velocities of the two H atoms in C_2H_2^+ have been modified so that approximately two modes of asymmetric and symmetric H—C—C bending, respectively, are excited. The results are shown in Fig. 6.

Unfortunately, all three trajectories with the initial conditions selected here are non-reactive. The CH_4 molecule comes close to C_2H_2^+ , dances for a while, and then flees. Nevertheless, we may make some observations on the dynamical processes based on these results. First, by comparing the results of the third and the first trajectory, we see that the symmetric H—C—C bending does not have much effect on the ‘reaction’ process. The H—C—C bending is nearly adiabatic in the whole process. This may not be very surprising considering the ‘symmetry’ of this trajectory. We expect a larger effect for cases with non-zero impact parameters.

Secondly, we see that trajectory 2, with the initial asymmetric bending excitation reveals interesting features of the process. Although the trajectory starts with a nearly symmetric configuration, CH_4 favours one carbon atom in C_2H_2^+ as it propagates, and forms the configuration that resembles **abs-1**. Clearly, the H—C—C asymmetric bending mode is far from being adiabatic and participates the ‘reaction’ process actively. It is also noted that the C—H bond that needs to be broken for reaction has been significantly stretched compared to the other two trajectories, and has been as long as 1.3 Å. At the same time, the C—H bond that needs to be formed has been as short as 1.15 Å, whereas, in other trajectories, the closest contact was only 1.45 Å. In other words, the second trajectory is nearly reactive. Clearly, the initial excitation of the asymmetric bending in C_2H_2^+ makes it easier to form the highly asymmetric classical complex **abs-1**, which is a critical step in the H-abstraction channel.

2.2.2 Conclusions. High quality *ab initio* calculations have been carried out to study the mechanism of the ion–molecule reaction $\text{CH}_4 + \text{C}_2\text{H}_2^+$. Compared with the previous work of Klippenstein,²² very similar profile of the H-abstraction channel (9) was obtained, despite some delicate differences. No entrance or exit barrier was found, and the reaction proceeds through a moderately bound (*ca.* 15 kcal mol⁻¹) intermediate complex. For the complex channel (7) and (8), a new transition state, **com-TS1**, with a C_1 structure has been located. The geometry and energetics of this structure are more consistent with experimental findings, and it is expected that, qualitatively, a correct cross-section can be derived using the results of the current work. Direct trajectory calculation reveals that asymmetric H—C—C bending participates in the reaction actively.

The authors are grateful to Prof. Joel M. Bowman and Prof. Steven J. Klippenstein for collaboration in the non-adiabatic TST project. This work was, in part, supported by Grants F49620-95-1-0182 and F49620-98-1-0063 from the Air Force Office of Scientific Research.

References

- 1 J. A. Miller and C. T. Bowman, *Prog. Energy Combust. Sci.*, 1989, **15**, 287.
- 2 For a recent summary of experimental work, see J. W. Bozzelli, M. H. U. Karim and A. M. Dean, *Proceedings of the 6th Toyota Conference on Turbulence and Molecular Processes in Combustion* (Elsevier, New York, 1993).
- 3 (a) M. R. Manaa and D. R. Yarkony, *J. Chem. Phys.*, 1991, **95**, 1808; (b) M. R. Manaa and D. R. Yarkony, *Chem. Phys. Lett.*, 1991, **188**, 352.
- 4 J. M. L. Martin and P. R. Taylor, *Chem. Phys. Lett.*, 1993, **209**, 143.
- 5 S. P. Walch, *Chem. Phys. Lett.*, 1993, **208**, 214.
- 6 (a) T. Seideman and S. P. Walch, *J. Chem. Phys.*, 1994, **101**, 3656; (b) T. Seideman, *J. Chem. Phys.*, 1994, **101**, 3662.
- 7 (a) See *e.g.* J. C. Lorquet and B. Leyh-Nihant, *J. Phys. Chem.*, 1988, **92**, 4778; (b) A. J. Marks and D. L. Thompson, *J. Chem. Phys.*, 1992, **96**, 1911; (c) S. Hammes-Schiffer and J. Tully, *J. Chem. Phys.*, 1995, **103**, 8528; (d) E. J. Heller and R. C. Brown, *J. Chem. Phys.*, 1983, **79**, 3336; (e) G. E. Zahr, R. K. Preston and W. H. Miller, *J. Chem. Phys.*, 1975, **62**, 1127.
- 8 A. M. Mebel, K. Morokuma and M. C. Lin, *J. Chem. Phys.*, 1995, **103**, 7414.
- 9 A. B. Baboul and H. B. Schlegel, *J. Chem. Phys.*, 1997, **107**, 9413.
- 10 (a) J. C. Keck, *Adv. Chem. Phys.*, 1967, **13**, 85; (b) W. H. Miller, *J. Chem. Phys.*, 1974, **61**, 1823.

- 11 For a review, see *e.g.* D. R. Yarkony, in *Modern Electronic Structure Theory*, ed. D. R. Yarkony, World Scientific, Singapore, 1995.
- 12 (a) N. Koga and K. Morokuma, *Chem. Phys. Lett.*, 1985, **119**, 371; (b) Q. Cui, Ph.D. Thesis, Emory University, 1997.
- 13 M. J. Bearpark, M. A. Robb and H. B. Schlegel, *Chem. Phys. Lett.*, 1994, **223**, 269.
- 14 W. H. Miller, N. C. Handy and J. E. Adams, *J. Chem. Phys.*, 1980, **72**, 99.
- 15 S. Kato, R. L. Jaffe, A. Komonicki and K. Morokuma, 1983, **78**, 4567.
- 16 W. H. Miller, *J. Chem. Phys.*, 1976, **65**, 2216.
- 17 A. S. Rodgers and G. P. Smith, *Chem. Phys. Lett.*, 1996, **253**, 313.
- 18 J. Qian, H. Fu and S. L. Anderson, *J. Phys. Chem.*, 1997, **101**, 6504.
- 19 (a) Y. Chiu, H. Fu, J. Huang and S. L. Anderson, *J. Chem. Phys.*, **102**, 1119; (b) Y. Chiu, H. Fu, J. Huang and S. L. Anderson, *J. Chem. Phys.*, 1994, **101**, 5410; (c) R. D. Guettler, G. C. Jones Jr., L. A. Posey and R. N. Zare, *Science*, 1994, **266**, 259.
- 20 G. Bouchoux, F. Penaud-Berruyer and M. T. Nguyen, *J. Am. Chem. Soc.*, 1993, **115**, 9728.
- 21 See, *e.g.* (a) A. Singa, M. C. Hsiao and F. F. Crim, *J. Chem. Phys.*, 1990, **92**, 6333; (b) A. Singa, M. C. Hsiao and F. F. Crim, *J. Chem. Phys.*, 1991, **94**, 4928; (c) M. J. Bronikowski, W. R. Simpson, B. Girard and R. N. Zare, *J. Chem. Phys.*, 1991, **95**, 8647; (d) A. Sinha, J. D. Thoenke and F. F. Crim, *J. Chem. Phys.*, 1992, **96**, 372; (e) S. S. Brown, R. B. Metz, H. L. Berghout and F. F. Crim, 1996, **105**, 6293; (f) S. S. Brown, R. B. Metz, H. L. Berghout and F. F. Crim, 1996, **105**, 8103; (g) R. P. Schmid, T. Arusi-Parpar, R.-J. Li, I. Bar and S. Rosenwaks, *J. Chem. Phys.*, 1997, **107**, 385 and references therein.
- 22 S. J. Klippenstein, *J. Chem. Phys.*, 1996, **104**, 5437.
- 23 L. A. Curtiss, K. Raghavachari, G. W. Trucks and J. A. Pople, *J. Chem. Phys.*, 1991, **94**, 7221.
- 24 See *e.g.* (a) R. Car and M. Parrinello, *Phys. Rev. Lett.*, 1985, **55**, 2471; (b) B. Hartke and E. A. Carter, *J. Chem. Phys.*, 1992, **97**, 6596; (c) V. Keshari and Y. Ishikawa, *Chem. Phys. Lett.*, 1994, **218**, 406; (d) A. I. Krylov and R. B. Gerber, *J. Chem. Phys.*, 1997, **106**, 6574; (e) M. S. Gordon, G. C. Chaban and T. Kaketsugu, *J. Phys. Chem.*, 1996, **100**, 11512.
- 25 (a) K. Fukui, *J. Phys. Chem.*, 1970, **74**, 23; (b) K. Fukui, S. Kato and H. Fujimoto, *J. Am. Chem. Soc.*, 1974, **97**, 1; (c) K. Fukui, *Acc. Chem. Res.*, 1981, **14**, 363.